Progress In Electromagnetics Research C, Vol. 75, 75–86, 2017

Multi-Band Omnidirectional Antenna with Hexagonal Prism Shape for MIMO Applications

Jiang-Yu Wang, Tao Tang*, and Run-Lin Zhang

Abstract—A multi-band antenna with omnidirectional radiation performance is proposed, which consists of 9 elements to form the structure of hexagonal prism. According to the placement rule, the antenna elements can be divided into two groups, one of which is placed in parallel on spaced three surfaces of the prism and the other placed vertically on the remaining spaced three faces of the prism. Each parallel element consists of two coplanar microstrip radiating patches which are nested within each other for miniaturization. Two parallel microstrips connected by a grounded disc with shorting pin are placed between the two patches to optimize the isolations. Each vertical element consists of two improved dipoles with four arms and a BALUN located at the back of the substrate plate which constitutes the quasi-Yagi structure. The resonant frequencies of the proposed prismatic antenna are 3.45 GHz, 4.9 GHz, 5.8 GHz and 15.2 GHz which can be used for low frequency bands of the fifth generation (5G) wireless communications and wireless local area networks (WLAN) as well as satellite communication applications.

1. INTRODUCTION

In the past few years, the mobile communication industry has developed from analog to digital 2G (GSM) to 3G and 4G (LTE). The 5G is going on and expected to be initiated by 2020 [1] to provide extremely high data rate for multimedia applications and internet of things (IoT).

There are two main directions of the development for 5G technologies: millimeter wave (mmW) [2] and MIMO [3]. The MIMO with large number of base station antennas on the transmitting and receiving ends can maximize the channel capacity for delivering high data.

However, due to the increase in the number of antenna elements for MIMO applications, such as the massive MIMO and full dimension MIMO (FD-MIMO) [4, 5] systems, the isolation between radiation elements becomes a key factor that will affect the MIMO's performance. The most direct way to reduce the coupling between ports is to increase the spacing between the elements. But it presents challenges for the structure size of design, which is how to structure enough antennas within a compact size.

Existing researches have presented some compact MIMO. An 18-port MIMO has been proposed in [6] which consists of six tri-polarization antenna elements with three ports mounted on six faces of a cube. A dual-band dual-polarized compact bowtie dipole antenna array for MIMO WLAN is proposed in [7], which consists of 12 antenna elements. Ref. [8] presents a tri-port MIMO antenna composed of three interconnected X-shaped arms.

Several methods have been proposed to improve the isolation of multi-antenna system [9, 10], including orthogonal placement of the antenna elements [11], separating the elements with additional structure or slits, such as EBG [12], and using network between elements.

In this paper, a hexagonal prism shaped 9-port MIMO antenna is proposed, in which resonant frequencies are 3.45 GHz, 4.9 GHz, 5.8 GHz and 15.2 GHz. It can be used for 5G communications

Received 31 March 2017, Accepted 26 May 2017, Scheduled 15 June 2017
* Corresponding author: Tao Tang (tangt@cuit.edu.cn).
The authors are with the College of Electronic Engineering, Chengdu University of Information Technology, Chengdu 610225, China.

and the WLAN as well as the Ku satellite communication bands applications. The maximum gain is 6.3 dBi, 5.3 dBi, 6.8 dBi and 7.8 dBi in each band. Due to the hexagonal prism structure of the antenna, omnidirectional radiation characteristics can be obtained. We begin with the design of the antenna, and the isolation optimization will be explained in Sections 2 and 3. Results are given in Section 4. Finally, conclusions are drawn in Section 5.

2. ANTENNA DESIGN

The proposed prism antenna consists of 9 microstrip antenna elements with 9 ports, which can be divided into two groups according to the placement rule. One group consists of three coplanar dual-port microstrip antennas placed in parallel on spaced three surfaces of the prism, and the other consists of three four-arm dipoles placed vertically on the remaining spaced three faces.

Each coplanar dual-port microstrip antenna consists of two nested radiation patches, corresponding to two operation frequency bands. Each four-arm dipole consists of two improved planar dipoles, located on the front and back sides of the substrate plate, respectively. It also corresponds to two operation frequency bands. All antenna elements are printed on a 1.5 mm thick Teflon substrate, whose relative permittivity is 2.1, and dielectric loss tangent is 0.001.

The configuration of the antenna is illustrated in Fig. 1. The vertical placement antennas are named V_1, V_2 and V_3, and the parallel placement antennas are denoted by P_s and P_b, in which P_{s1}, P_{s2} and P_{s3} refer to the smaller patches of each coplanar dual-port microstrip antenna operating in 15.2 GHz bands, but P_{b1}, P_{b2} and P_{b3} refer to the larger patches of each coplanar dual-port microstrip antenna operating in 5.8 GHz bands. P_s and P_b patches are nested within each other for reducing the overall size.

The dual polarizations can be obtained with the vertical placement elements providing vertical polarization and the parallel placement elements providing horizontal polarization.

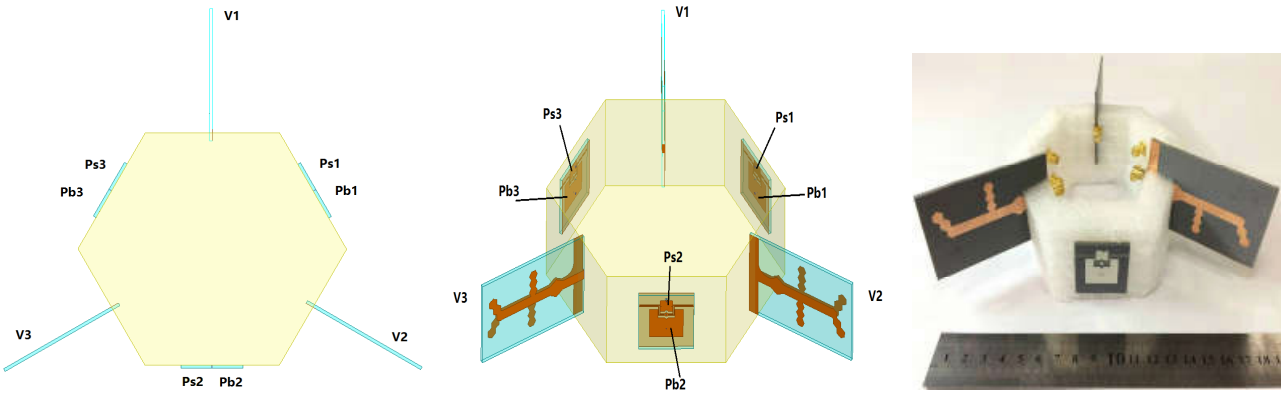

(a) (b) (c)

Figure 1. Configuration of the proposed antenna. (a) Top view. (b) 3D view. (c) Photo.

2.1. Coplanar Dual-Port Microstrip Antenna

Each parallel placement antenna element consists of two patches, denoted P_s and P_b corresponding to 15.2 GHz and 5.8 GHz bands, and their sizes are respectively 0.36λ and 0.37λ. The operation bands cover part of the WLAN bands and Ku satellite communication bands [13]. A C-shaped slot is arranged on the patch P_b to increase the bandwidth, and P_s can be nested in the C-shaped slot in order to reduce the overall size of the elements. Both patches are fed by coaxial probe.

Two parallel microstrip lines connected by a grounded disc with shorting pin are placed between the two patches, and two slots are arranged on the vertical sides of the small patches P_s. The configuration is shown in Fig. 2, and the specific size of each part is given in Table 1.

Table 1. Detailed size of coplanar dual-port microstrip antenna (unit: mm).

W_{p1}	L_P	W_{p2}	H_{p1}	H_{P2}	W_{p3}
12	5.04	9.46	1.68	0.5	3.65
H_{p3}	F_p	K_p	R_{P1}	R_{p2}	
0.1	0.78	0.25	1	1.3	

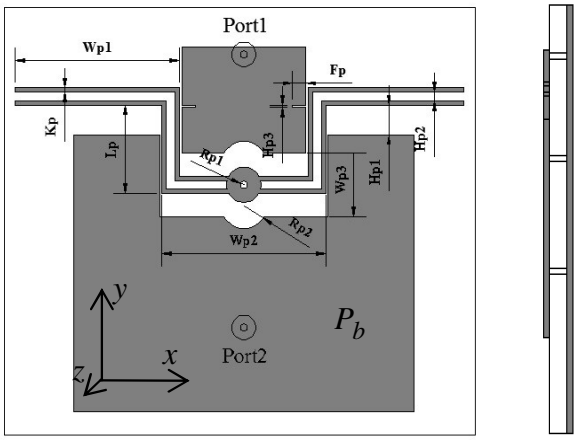

(a) (b)

Figure 2. Geometries of the coplanar dual-port microstrip antenna. (a) Top view. (b) Side view.

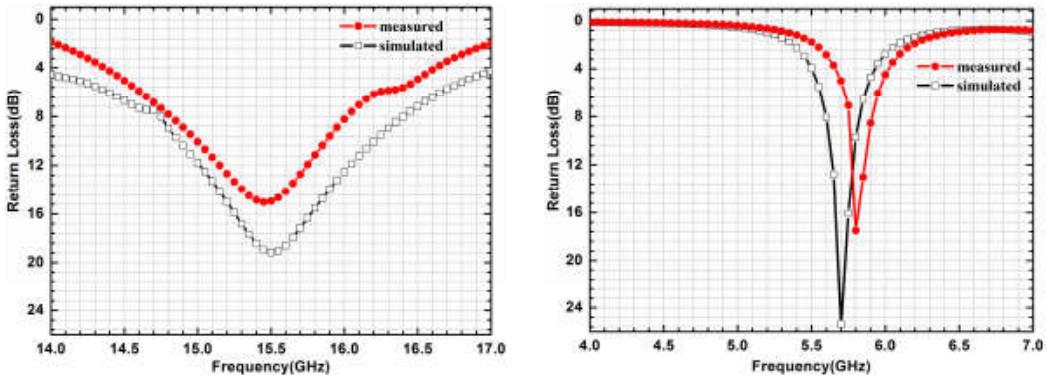

(a) (b)

Figure 3. Return loss. (a) Port 1. (b) Port 2.

The return loss and radiation patterns of the coplanar dual-port microstrip antenna are shown in Fig. 3 and Fig. 4. And the measured and simulated gains are plotted in Figs. 5(a) and (b).

2.2. Four-Arm Dipole

As shown in Fig. 6, each four-arm dipole consists of two improved planar dipoles, and the radiation arms are located in the front and back of the substrate plate. The lengths of short-arm and long-arm are 0.42λ and 0.38λ corresponding to 4.9 GHz and 3.45 GHz, respectively.

Each arm of the four-arm dipole is constructed of a series of hexagonal microstrip structures. Symmetrical microstrip lines located on the front and back sides of the substrate are used for feeding. A hexagonal structure is located on the symmetrical feed lines to adjust the input impedance. A

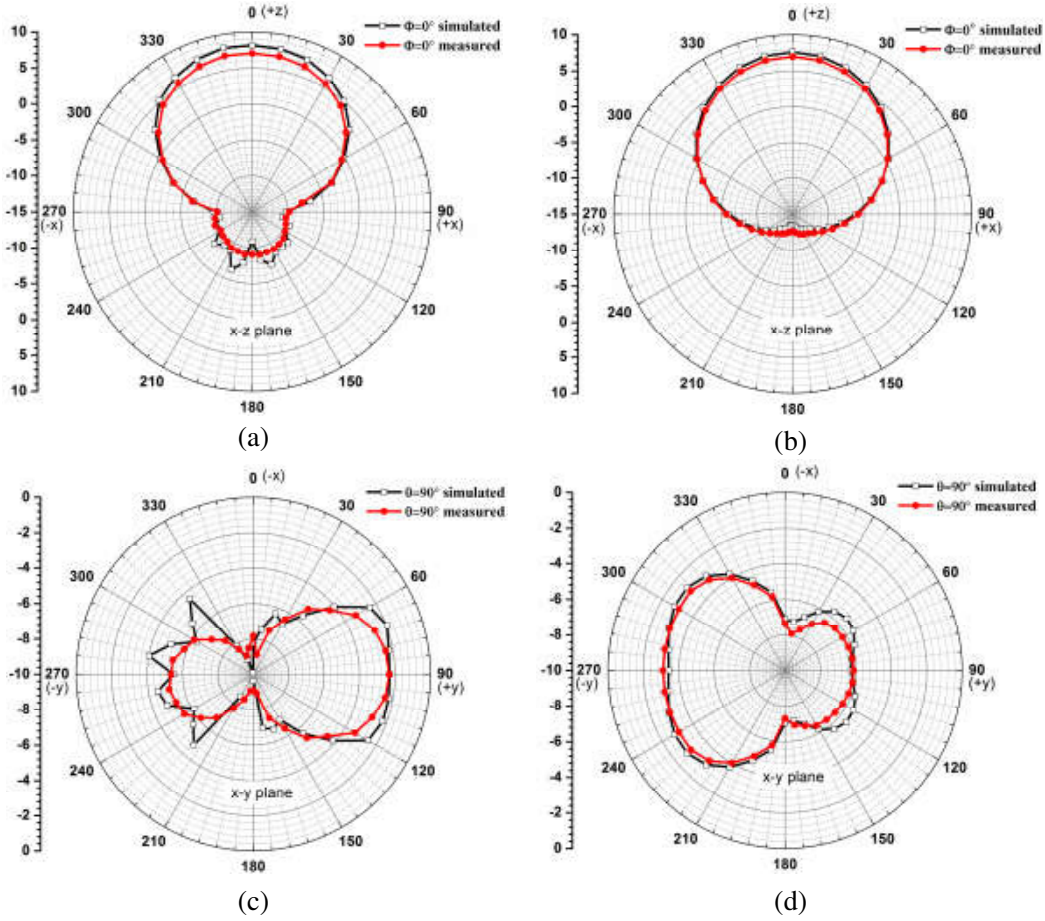

Figure 4. Radiation pattern. (a) E-plane of port 2. (b) E-plane of port 1. (c) H-plane of port 2. (d) H-plane of port 1.

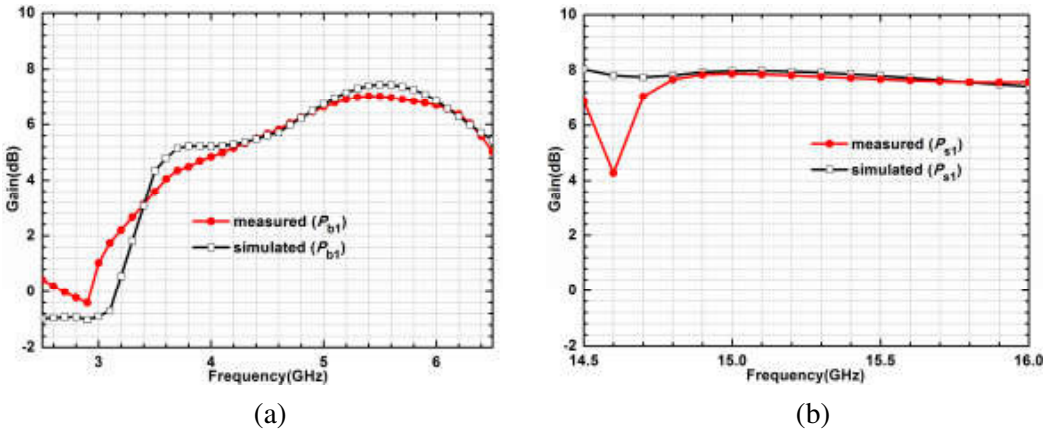

Figure 5. Gain of the coplanar dual-port microstrip antenna.

BALUN is set at the end of the front feed line to improve the matching and also provides the function of a reflector for the entire antenna.

In order to reduce the impact of the front arms on the back in radiation performance, the arms of the front dipole are placed in a V-shape. Table 2 gives the detailed size of the dipole. Moreover, the four-arm dipole antenna has a quasi-Yagi structure, and its radiation performance is similar to Yagi

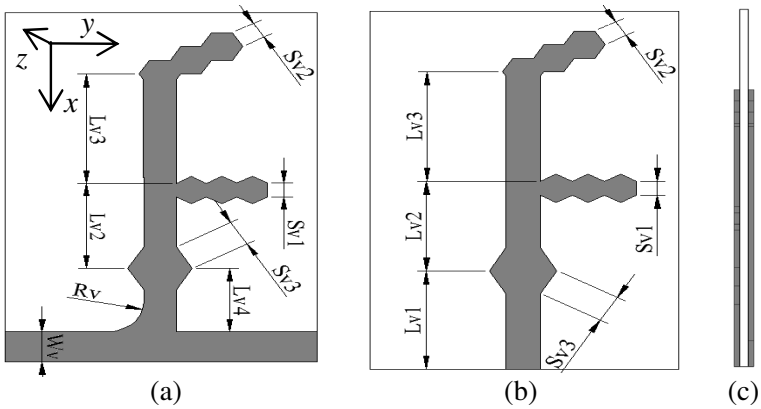

Figure 6. Geometry of four-arm dipole antenna. (a) Top view. (b) Back view. (c) Side view.

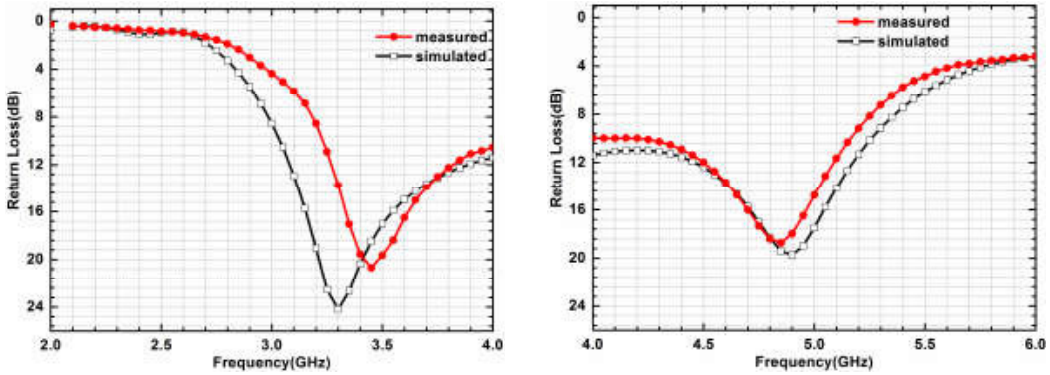

Figure 7. Return loss. (a) 3.45 GHz. (b) 4.9 GHz.

Table 2. Detailed size of four-arm dipole (unit: mm).

L_{v1}	L_{v2}	L_{v3}	L_{v4}	S_{v1}
18.6	16.88	20.56	12.6	2.69
S_{v2}	S_{v3}	R_v	W_v	
2.97	4.93	5.6	6	

antenna.

According to IMT-2020 (5G), C-band is one of the candidates for 5G in China [14, 15], which includes 3.3–3.6 GHz, 4.4–4.5 GHz, 4.8–4.99 GHz. Therefore, the operation bands of the proposed four-arm dipole cover part of 5G low frequency bands.

Figures 7 and 8 show the return loss and radiation patterns of the four-arm dipole antenna, and the measured and simulated gains are given in Fig. 9.

3. ISOLATION OPTIMIZATION

As shown in Fig. 2, in order to obtain a miniaturization design, the radiation patches of the coplanar dual-port microstrip antenna are nested within each other, but this structure will bring serious coupling between P_s and P_b. In order to improve the port isolation, two parallel microstrip lines are designed

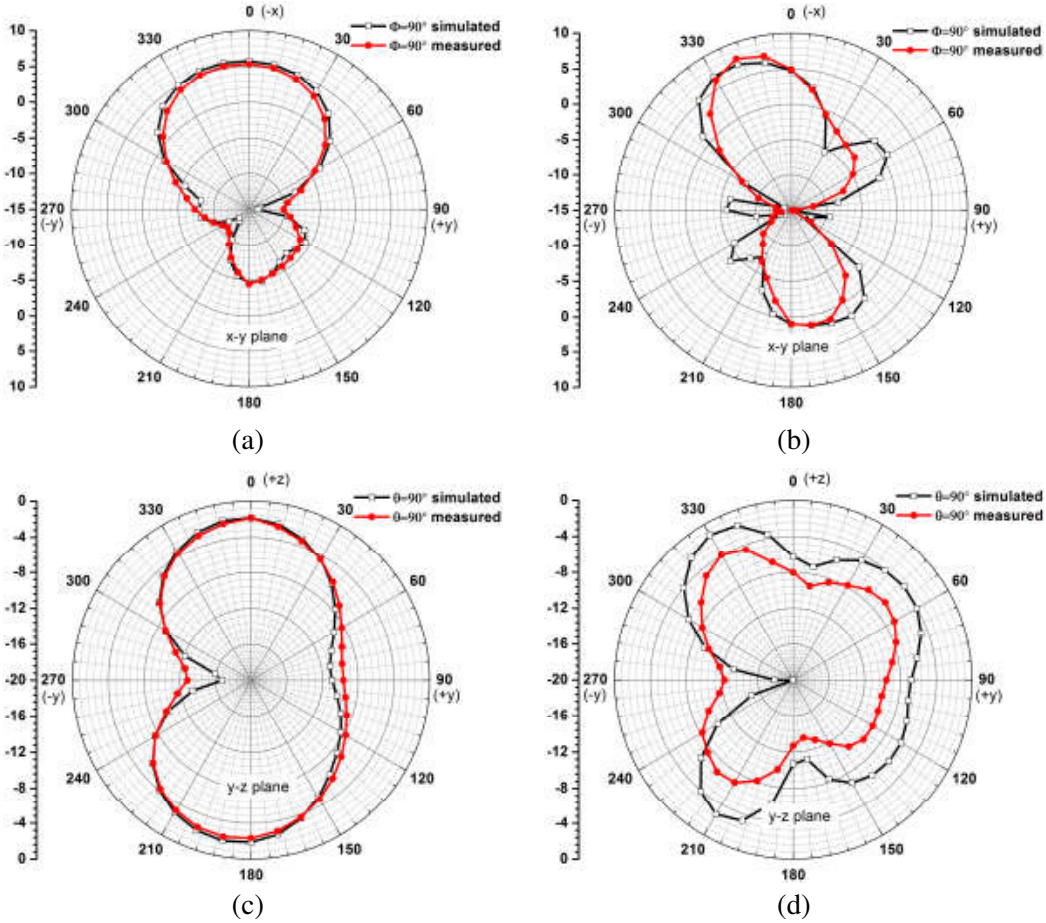

Figure 8. Radiation pattern. (a) E-plane of 3.45 GHz. (b) E-plane 4.9 GHz. (c) H-plane of 3.45 GHz. (d) H-plane of 4.9 GHz.

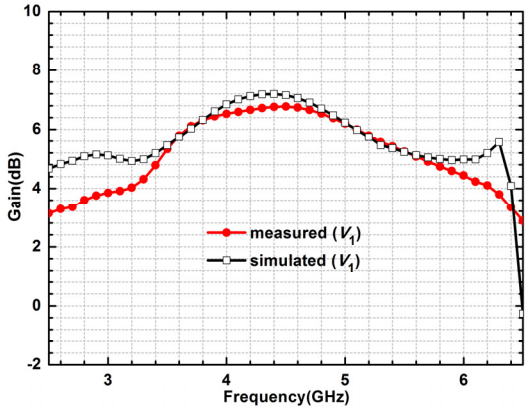

Figure 9. Gain of the four-arm dipole.

between two patches to isolate the coupling current. The coupling current distributions on P_s and P_b are given in Figs. 10(a) and (b), from which, one can see that most of the coupling current is distributed on the parallel microstrip lines. Isolation of the port in this state is shown in Fig. 11(a) which shows that the introduction of parallel microstrip lines improves isolation of part of the low-frequency port, but the isolation in the entire low-frequency range does not meet the design requirements.

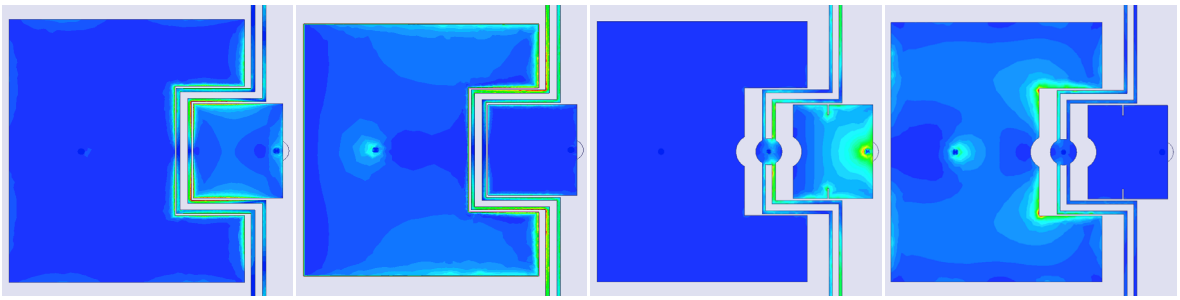

Figure 10. Coupling current distribution. (a) Feed by port 1 with two parallel microstrip lines. (b) Feed by port 2 with two parallel microstrip lines. (c) Feed by port 1 with two parallel microstrip lines, grounded disc and slots. (d) Feed by port 2 with two parallel microstrip lines, grounded disc and slots.

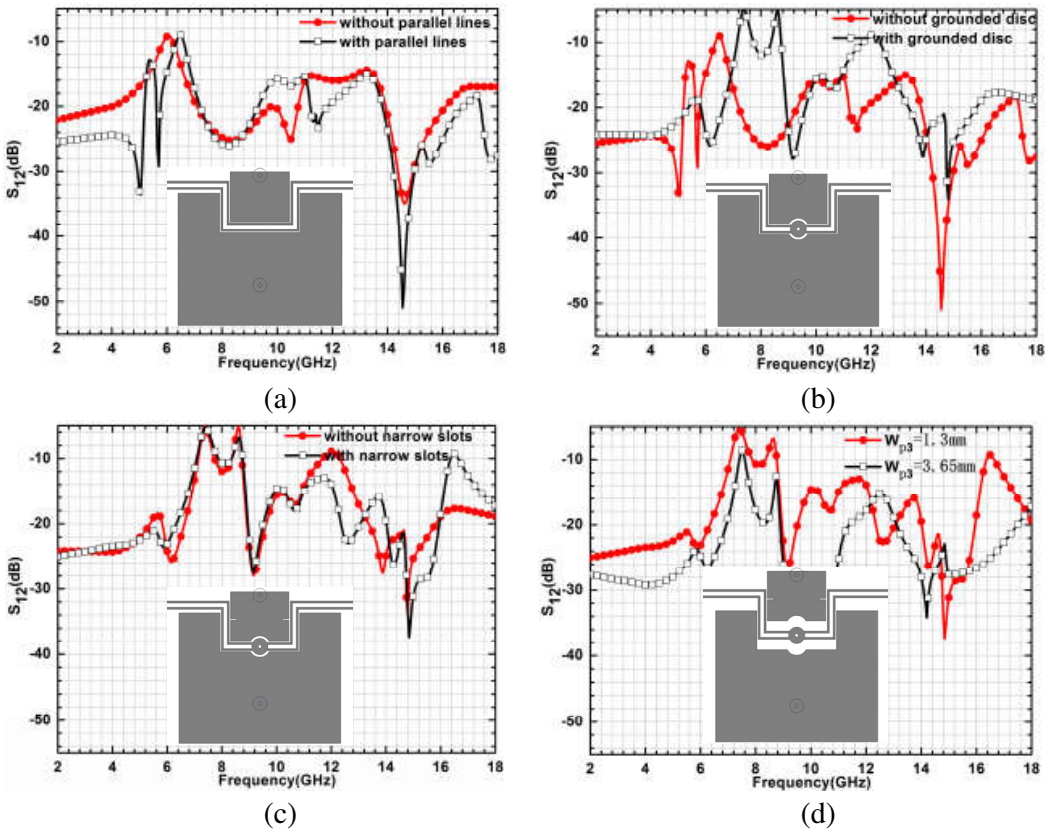

Figure 11. Isolation. (a) With and without the microstrip lines. (b) With and without the grounded disc. (c) With and without slots. (d) The longitudinal spacing W_{p3}.

The coupling current distributed on the parallel microstrip lines will affect the antenna radiation performance. To reduce this effect, a grounded disc with shorting pin is introduced and connected to the middle of the parallel microstrip lines. The ground plate, patches and dielectric substrate together form a waveguide, and the grounded disc redirects the radiation of the coupling surface wave along this waveguide to become backside radiation radiation so that coupling between antenna elements P_b and P_s is decreased [16].

As shown in Fig. 11(b), after introduction of the grounded disc, the isolation of the low frequency band is improved, but the high frequency band is deteriorated.

At the same time, it can be seen from Fig. 10(b) that the coupling current on the vertical side of the nested patch corresponds to port 1 is still large. To reduce this effect, two slots are introduced on the vertical sides of the nested patch to modify the current path, which is equivalent to increasing the two patch spacing.

Figure 11(c) shows the isolation after the introduction of parallel microstrip lines, grounded disc and two slots, which indicate that the isolations both in the low and high frequency bands of the coplanar dual-port microstrip antenna are greater than 20 dB.

Finally, the longitudinal spacing of two patches W_{p3} is properly increased, making the port isolation further optimized. During all isolation optimization processes, the change in return loss of the two ports is small. The final coupling current is shown in Figs. 10(c) and (d), and the final optimized port isolation is given in Fig. 11(d). From Figs. 10(c) and (d), one can note that the coupling current is almost non-existent after optimization.

Arrangement and placement of the elements in an appropriate manner can effectively improve the isolation of the entire hexagonal prism shaped antenna. Fig. 12 shows the current distribution, from which it can be seen that there are virtually no coupling current flows to the other antennas when vertical positioning elements and parallel elements are excited individually.

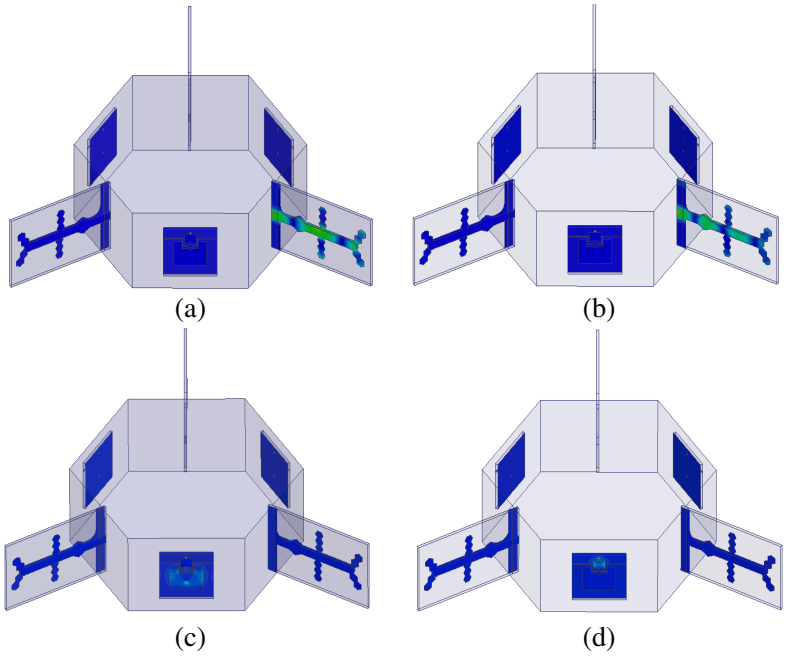

Figure 12. Current distribution of the proposed array. (a) V_2 excited at 3.45 GHz. (b) V_2 excited at 4.9 GHz. (c) P_{b2} excited at 5.8 GHz. (d) P_{s2} excited at 15.2 GHz.

4. RESULTS FOR THE HEXAGONAL PRISM SHAPED ANTENNA

Due to the symmetry of the proposed hexagonal prism shaped antenna, the isolation between any two of the 9 antenna elements can be indicated by $|S_{V_1V_2}|$, $|S_{V_1P_{s1}}|$, $|S_{V_1P_{b1}}|$, $|S_{V_1P_{s2}}|$, $|S_{V_1P_{b2}}|$, $|S_{P_{s1}P_{s2}}|$, $|S_{P_{b1}P_{b2}}|$, $|S_{P_{s1}P_{b1}}|$ and $|S_{P_{s1}P_{b2}}|$. The measured S-parameters in Fig. 13 show that all the isolations between any two ports are greater than 20 dB.

Due to the vertical placement elements providing vertical polarization and the parallel placement elements providing horizontal polarization, the vertical and parallel antennas exhibit low cross-polarization in 3.45 GHz, 4.9 GHz, 5.8 GHz and 15.2 GHz bands, which can be seen in Fig. 14.

Due to its hexagonal prism structure, the omnidirectional radiation characteristic can be obtained. The radiation patterns of the entire antenna are given in Fig. 15.

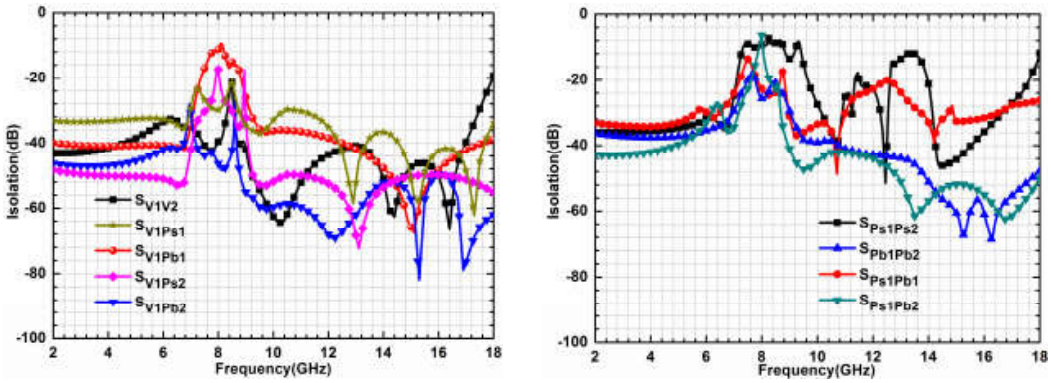

Figure 13. Isolation of the antenna. (a) Between one of the vertical elements and the other elements. (b) Between the parallel elements.

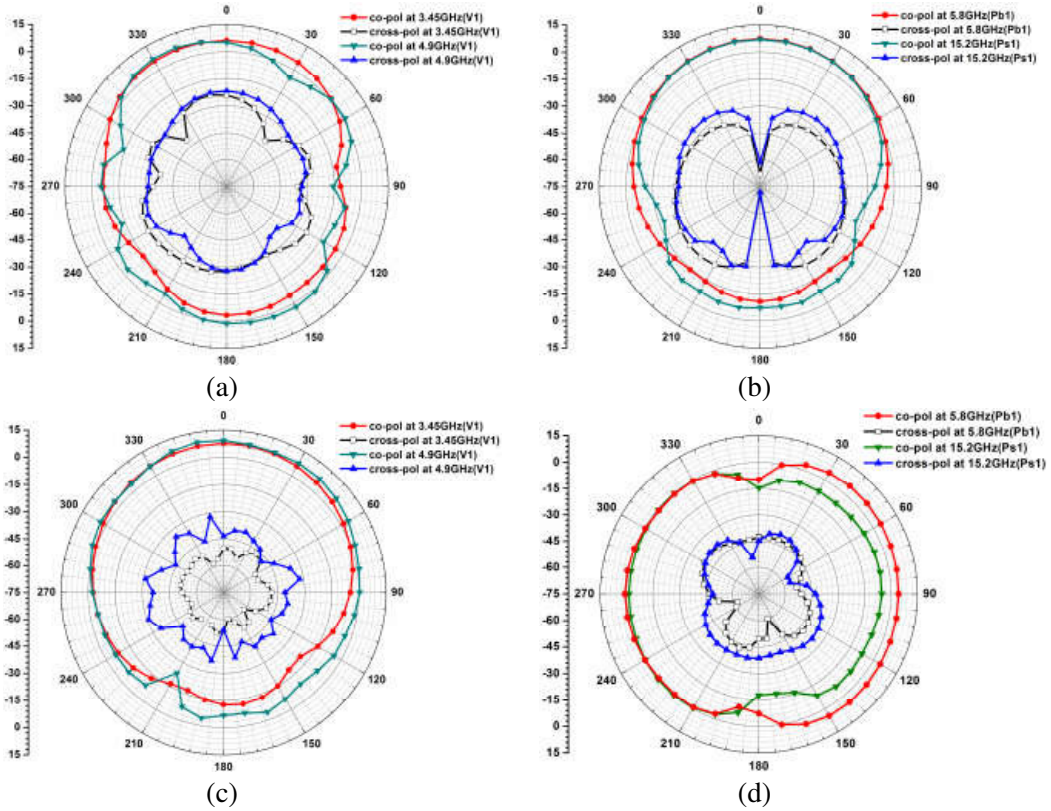

Figure 14. Co-polarization and cross-polarization radiation at 3.45 GHz, 4.9 GHz, 5.8 GHz and 15.2 GHz. (a) E-plane of 3.45 GHz and 4.9 GHz. (b) E-plane of 5.8 GHz and 15.2 GHz. (c) H-plane of 3.45 GHz and 4.9 GHz. (d) H-plane of 5.8 GHz and 15.2 GHz.

The envelope correlation coefficients (ECC) show a diversity behavior of MIMO, which involves all the S parameters of the designed MIMO antenna. Lower value of ECC means lower correlation between antenna elements. The ECC of the proposed antenna can be calculated by the S-parameters [17, 18]

$$\rho_e = \frac{\left|S_{11}^* S_{12} + S_{21}^* S_{22}\right|^2}{\left(1 - \left|S_{11}\right|^2 - \left|S_{21}\right|^2\right)\left(1 - \left|S_{22}\right|^2 - \left|S_{12}\right|^2\right)} \tag{1}$$

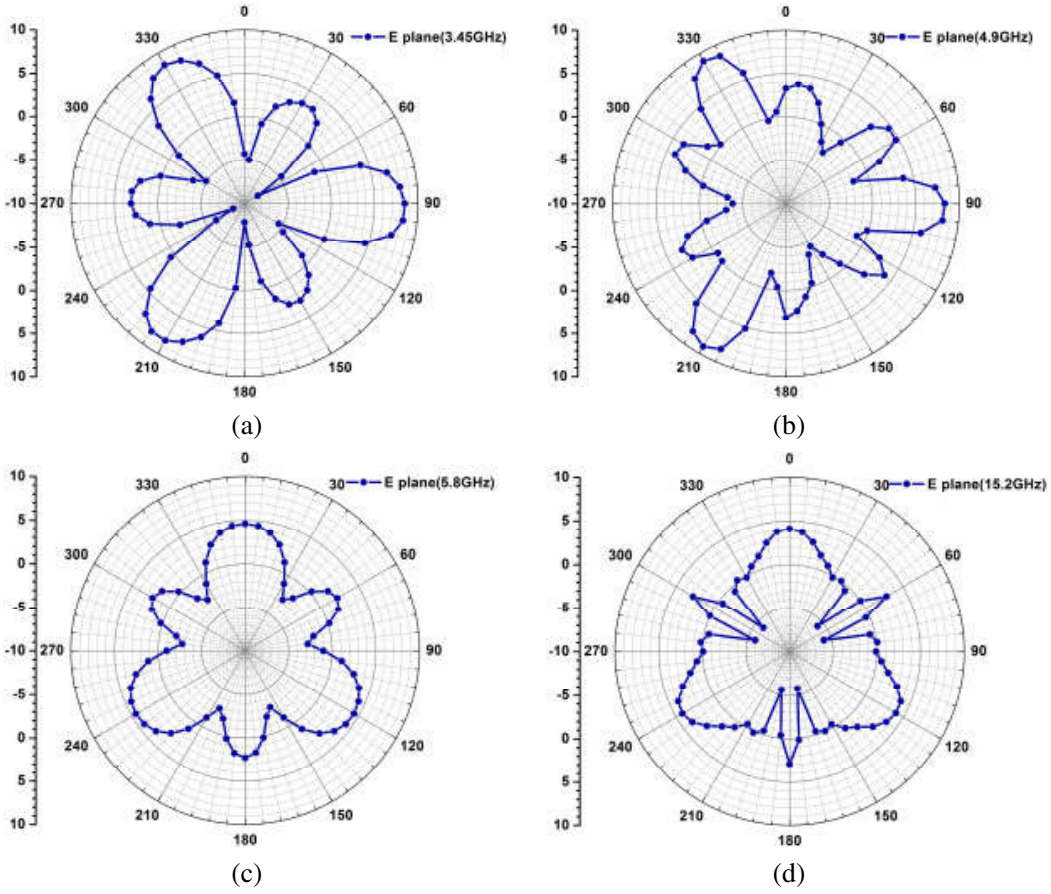

Figure 15. The radiation patterns of the hexagonal prism shaped antenna. (a) 3.45 GHz. (b) 4.9 GHz. (c) 5.8 GHz. (d) 15.2 GHz.

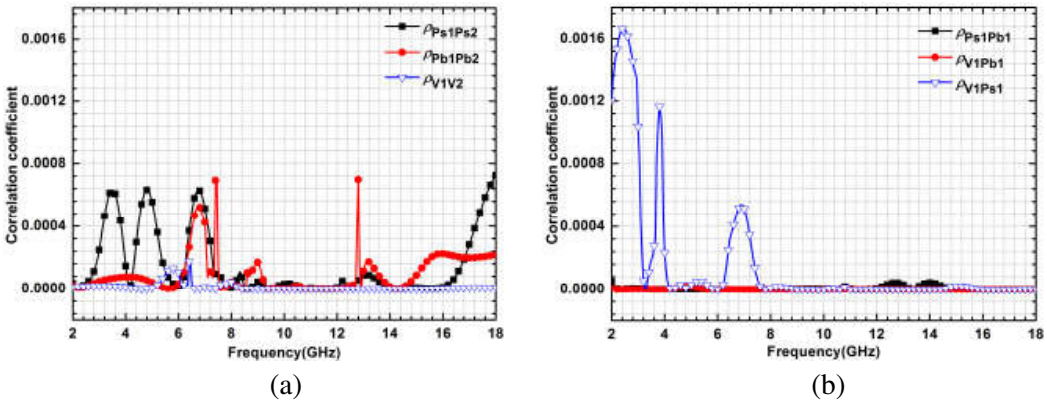

Figure 16. Correlation coefficients. (a) ECCs of the (P_{s1}, P_{s2}), (P_{b1}, P_{b2}) and (V_1, V_2). (b) ECCs of the (P_{s1}, P_{b1}), (V_1, P_{b1}) and (V_1, P_{s1}).

As shown in Fig. 16, all the ECCs of the proposed antenna are under 1.7e-3 in the bands of interest, indicating a good MIMO performance. Note that the larger the distance is between two ports, the lower ECC the results indicate [7]. Therefore, Fig. 16 only shows the ECCs of the antenna elements close to each other, which are sufficient to evaluate all the ECCs of the prism antenna.

5. CONCLUSIONS

A novel MIMO antenna with 9 elements and four operating bands for 5G and WLAN as well as Ku band applications is reported. The overall structure of the antenna is a hexagonal prism.

The antenna elements are placed parallel and vertically on surfaces of the prism, respectively. Parallel microstrip lines, grounded disc and slots are used to improve port isolations of the nested antennas. The proposed antenna provides an omnidirectional radiation characteristic due to its prismatic structure.

The results show that the resonant frequencies of the proposed MIMO are 3.45 GHz, 4.9 GHz, 5.8 GHz and 15.2 GHz, and the maximum gains is 6.3 dBi, 5.3 dBi, 6.8 dBi and 7.8 dBi in each band. It can be used for low frequency bands of 5G and WLAN as well as the Ku bands satellite communication applications.

ACKNOWLEDGMENT

This work was supported by the Sichuan Science and Technology Supporting Project (Nos. 2015GZ0282, 2017GZ0300).

REFERENCES

1. Patel, S., C. Malhar, and K. Kinjal, "5G: Future mobile technology-vision 2020," *International Journal of Computer Applications*, Vol. 54, No. 17, 6–10, 2012.
2. Sun, C. C. and H. T. Chou, "Summary and progress of MM-wave antenna technologies for 5G application," *2016 IEEE International Symposium on Radio-Frequency Integration Technology*, 1–3, 2016.
3. Ji, H., Y. Kim, J. Lee, E. Onggosanusi, Y. Nam, J. Zhang, B. Lee, and B. Shim, "Overview of full-dimension MIMO in LTE-advanced pro," *IEEE Communications Magazine*, Vol. 99, 2–11, 2016.
4. Kim, Y., H. Ji, J. Lee, Y. H. Nam, B. L. Ng, I. Tzanidis, Y. Li, and J. Zhang, "Full dimension MIMO (FD-MIMO): The next evolution of MIMO in LTE systems," *IEEE Wireless Communications*, Vol. 21, No. 2, 26–33, 2014.
5. Gao, Y., R. Ma, Y. Wang, Q. Zhang, and C. Parini, "Stacked patch antenna with dual-polarization and low mutual coupling for massive MIMO," *IEEE Transactions on Antennas and Propagation*, Vol. 64, No. 10, 4544–4549, 2016.
6. Zheng, J., X. Gao, and Z. Zhang, "A compact eighteen-port antenna cube for MIMO systems," *IEEE Transactions on Antennas and Propagation*, Vol. 60, No. 2, 445–455, 2012.
7. Zheng, W. C., L. Zhang, Q. X. Li, and Y. Leng, "Dual-band dual-polarized compact bowtie antenna array for anti-interference MIMO WLAN," *IEEE Transactions on Antennas and Propagation*, Vol. 62, No. 1, 237–246, 2014.
8. Wang, H., L. S. Liu, Z. J. Zhang, "A tri-port MIMO antenna designed for micro/pico cell applications with self-decoupled structure," C*hina Communications*, Vol. 11, No. 11, 1–6, 2014.
9. Bouezzeddine, M. and W. L. Schroeder, "Design of a wideband, tunable four-port MIMO antenna system with high isolation based on the theory of characteristic modes," *IEEE Transactions on Antennas and Propagation*, Vol. 64, No. 7, 1–1, 2016.
10. Malekpour, N. and M. A. Honarvar, "Design of high-isolation compact MIMO antenna for UWB application," *Progress In Electromagnetics Research C*, Vol. 62, 119–129, 2016.
11. Luo, Y., Q. Chu, J. Li, and Y. Wu, "A planar H-shaped directive antenna and its application in compact MIMO antenna," *IEEE Transactions on Antennas and Propagation*, Vol. 61, No. 9, 4810–4814, 2013.
12. Hsu, C., K. Lin, and H. Su, "Implementation of broadband isolator using metamaterial-inspired resonators and a T-shaped branch for MIMO antennas," *IEEE Transactions on Antennas and Propagation*, Vol. 59, No. 10, 3936–3939, 2011.

13. Novak, M. H. and J. L. Volakis, "Ultrawideband antennas for multiband satellite communications at UHF-Ku frequencies," *IEEE Transactions on Antennas and Propagation*, Vol. 63, No. 4, 1334–1341, 2015.
14. Tan, H., W. Li, T. Wang, J. Fang, and Z. Feng, "The analysis on the candidate frequency bands of future mobile communication systems," *China Communications*, 12 (Supplement), 140–149, 2015.
15. Wang, T., G. Li, J. Ding, and Q. Miao, "5G Spectrum: Is China ready," *IEEE Communications Magazine*, Vol. 53, No. 7, 58–65, 2015.
16. Alvey, G. R. and J. T. Bernhard, "Increasing isolation between multiple antennas with a grounded meander line structure" U.S. Patent, No. US7701395.2010, 2010.
17. Pan, Y., Y. Cui, and R. Li, "Investigation of a triple-band multibeam MIMO antenna for wireless access points," *IEEE Transactions on Antennas and Propagation*, Vol. 64, No. 4, 1234–1241, 2016.
18. Salonen, I. and P. Vainikainen, "Estimation of signal correlation in antenna arrays," *Proceedings of the 12th International Symposium on Antennas*, Vol. 2, 383–386, 2002.